

Article

Alternative Liquid-Assisted Sintering of Al/Cu Composites Using Selected Powders of As-Cast Al-Zn Alloy

Eder L. Ortiz ¹, Wislei R. Osório ², Ausdinir D. Bortolozo ^{1,2} and Giovana S. Padilha ^{1,*}

¹ School of Applied Sciences/FCA, Research Group in Manufacturing of Advanced Materials, University of Campinas (UNICAMP), Campus Limeira, 1300, Pedro Zaccaria Street, Jd. Sta Luiza, Limeira 13484-350, Brazil; ederlopesortiz@gmail.com (E.L.O.); ausdinir@unicamp.br (A.D.B.)

² School of Technology, University of Campinas (UNICAMP), Campus Limeira, Limeira 13484-332, Brazil; wislei1@unicamp.br

* Correspondence: giovanap@unicamp.br

Abstract: Al and its alloys constitute one of the most versatile, economical, and attractive materials for a wide range of applications. The 7xxx and 2xxx series alloys achieve the highest mechanical strength among the aluminum alloys. In this investigation, powder metallurgy is used to characterize the microstructural and mechanical properties of a noncommercial Al₆Cu₅Zn alloy. Initial powder sizes are determined, and the best conditions are obtained for distribution between 75 and 106 μm. The samples are sintered at 585 °C, 600 °C and 615 °C for 0.5, 1.5 h and 3 h. Similar mechanical behavior to that of the as-cast Al-Cu-based alloys is attained (~125 MPa) for the samples sintered at 615 °C for 3 h. In terms of a reduction in energy consumption and in the metal fumes commonly evidenced by foundry applications, Al-Zn powders have the potential to be associated with Al and Cu powders in an Al₆Cu₅Zn composite constitution.

Keywords: intermetallic phase; Al₆Cu₅Zn alloy; powder metallurgy and mechanical properties



Citation: Ortiz, E.L.; Osório, W.R.; Bortolozo, A.D.; Padilha, G.S.

Alternative Liquid-Assisted Sintering of Al/Cu Composites Using Selected Powders of As-Cast Al-Zn Alloy. *Metals* **2022**, *12*, 962. <https://doi.org/10.3390/met12060962>

Academic Editor: Elena Gordo

Received: 25 April 2022

Accepted: 28 May 2022

Published: 3 June 2022

Publisher's Note: MDPI stays neutral with regard to jurisdictional claims in published maps and institutional affiliations.



Copyright: © 2022 by the authors. Licensee MDPI, Basel, Switzerland. This article is an open access article distributed under the terms and conditions of the Creative Commons Attribution (CC BY) license (<https://creativecommons.org/licenses/by/4.0/>).

1. Introduction

Both the 7xxx and 2xxx series alloys are heat-treatable alloys, and high mechanical strengths can be reached. For this reason, these alloys are commonly used in the automotive and aircraft industries [1]. This encourages the research and development of new materials and manufacturing methods. Aluminum alloys are attractive for use in certain engine parts that benefit from a lighter structure and are more effective when compared to the materials that were previously employed. In addition, lighter and more efficient vehicles save energy; consequently, pollution is reduced with improved performance [1,2].

Although Al alloys exhibit a high strength-to-weight ratio, certain improvements in the mechanical properties with reinforcements are needed, and so new blends of Al alloys are being formed. The mechanical properties and applications of both automotive and aircraft parts made from Al alloys are affected by the content applied [1,3]. Metallic and nonmetallic elements, such as Fe, Cu, Pb, In, Zn, Ni, Mg, Si, Ti, and Sn, are responsible for improving the mechanical properties of Al-based commercial alloys [2,4–7]. When Zn content is utilized, a liquid phase formation in an Al-Cu binary system is formed [8]. This enhances the liquid phase, and the mechanical strength is increased. For this reason, when the liquid phase is located in pores, improving the adhesion of powders, the densification is increased and, consequently, an improvement in mechanical properties is also achieved [3,5,9,10].

As aforementioned, the 7xxx series (Al-Zn), 2xxx series (Al-Cu) and 6xxx and 5xxx (Al-Mg-Si) alloys are precipitation-hardening aluminum alloys. These alloys have their hardness values increased by the control of thermal treatment under specific conditions, i.e., solubilization and aging. The solvus temperatures of the 7xxx series alloys are relatively lower than those of other aluminum alloys [11].

Zinc itself is highly soluble in aluminum, and no appreciable influence on the microstructure takes place. However, a typical Al-Zn alloy commonly contains copper, chromium, manganese, and zirconium. Iron and silicon contents in the form of impurities are also detected. The precipitation hardening occurs in a sequence that begins with the formation of Guinier Preston zones (GP) from the supersaturated solid solution. Sequentially, the coherent metastable precipitates M' until reaching the phase of equilibrium with M . These phenomena occur in the over-aging stage, and a substantial decrease in hardness is observed [12].

Al-Cu system alloys, known as 2xxx (worked) and 2xx.x (cast) series alloys are the earliest developmental aluminum alloys. Their emergence dates back to the beginning of the twentieth century. Generally, Al-Cu alloys have high mechanical strength after precipitation-hardening heat treatment. However, despite this advantage, they have other disadvantages (e.g., corrosion resistance and limited castability) when compared with other aluminum alloys. The highest hardness values are obtained when copper contents ranging between 4% and 6% are used [12,13].

As previously mentioned, the Al-Cu alloys have high mechanical strength after precipitation hardening, due to GP zone formation. These are characterized by disk shapes formed by the arrangement of copper and aluminum atoms in the regions enriched by copper, increasing the resulting hardness. This precipitate is formed after a few hours, and it is coherent with the matrix in a plate-like shape. The continuation of the aging treatment leads to the formation of the equilibrium precipitate, corresponding with the stoichiometric of the Al_2Cu . This is called the thermodynamic equilibrium precipitate, since the continuation of aging has provided no further modification to its characteristics, except for the sizes of these particles, which tend to grow. The formation of this equilibrium precipitate also corresponds to so-called over-aging, where the hardness is decreased [14].

Both binary groups of Al-Zn and Al-Cu alloy systems have limitations. Their properties can be substantially improved by combining these elements in a blend of Al-Cu-Zn, which is basically a 7xxx series alloy. The Al-Cu liquid phase occurs at 548 °C, while the Al-Zn liquid phase occurs at 380 °C. In this way, the appropriate amount of Zn liquid phase within the melting temperature of Al favors the sintering conditions of Al [3,15]. Based on these previous investigations, it seems that when using an Al-Zn master alloy associated with elemental Al and Cu powders, a liquid phase is constituted and assisted-liquid sintering is provided [8].

The casting process has usually been adopted for the manufacture of aluminum alloy parts. In addition, centrifugal casting and shell molding are also used. The selection of the manufacturing route depends on several factors and aspects of the components adopted. The component size, shape and complexity, the physical and mechanical properties of the adopted alloy, and the minimum and maximum thicknesses of each section are some of the technical and operational aspects [16]. The economic factors are batch size and the relative costs of machining and finishing. Powder metallurgy (PM) is an alternative-manufacturing route associated with lower energy and materials consumption than is used for those components conventionally manufactured using traditional routes [17]. PM offers an economical method for improving the mechanical properties of aluminum alloys. However, some parameters should be optimized to achieve low manufacturing costs and beneficial properties. The utilization of powders obtained from ingots of Al-based alloys induces more economic and competitive manufacturing routes [5,18].

Based on the aforementioned factors, the aim of this investigation is focused on the evaluation of the effects of both specific sintering times (i.e., 0.5 h, 1.5 h and 3 h) and temperatures (at 585 °C, 600 °C and 615 °C) upon mechanical behavior. Additionally, scanning electron microscope with energy-dispersive X-ray spectroscopy (SEM-EDX) and X-ray diffraction (XRD) techniques are used to characterize the resulting microstructural arrays and phase to create the Al_6Cu_5Zn alloys examined.

2. Materials and Methods

A commercial Al ingot was used (0.11 wt % Fe, 0.06 wt % Zn, 0.02% wt % Mn; 0.009 wt % Cu; other <0.001 wt %). Electrolytic Cu and Zn ingots (99.90 wt %) were also used to obtain powder particles to create the Al₆Cu₅Zn alloy. An Al₂₀Zn master alloy was produced, utilizing Al and Zn powders to blend with other powders and the Al₆Cu₅Zn alloy samples that were created. This procedure was also applied in a previous investigation [3]. Additionally, this procedure is also carried out because Zn has a relatively low melting point, and, at certain sintering temperatures and periods, certain portions of Zn can evaporate considerably (and be lost). For this purpose, Al and Zn were melted at 600 °C for 15 min and the master alloy was produced. To create the Al₆Cu₅Zn alloy, amounts of Al, Cu and Al₂₀Zn powders were prepared using milling. Powders with particle sizes of between 75 and 106 µm were selected. The following powder proportions of Al and Cu and Al₂₀Zn were used: 1.035 g, 0.09 g and 0.375 g, respectively. Sequentially, these powders were mixed inside a mortar and pestle for ~5 min. A uniaxial hydraulic press (Marcon-MPH15, Marília, Brazil) giving a loading compaction of 10 ton was used. The mixed powders were placed inside a tempered steel die with an area of 270 mm² to proceed with the compaction process. Due to the raising of the environmental temperature, i.e., ~27 (± 2) °C up to 585 °C, 600 °C and 615 °C, applying a heating rate of 10 °C.min⁻¹, the compacted green samples (samples before heat treatment) under a pure nitrogen atmosphere were sintered. The sintering times of 0.5 h, 1.5 h and 3 h were adopted. When combining the sintering temperatures and times, nine distinct sintering conditions were attained and utilized. Subsequently, during the sintering stages, the samples were water-quenched at 27 (± 2) °C. A schematic representation of the powder metallurgy stages and sample synthesis are shown in the Graphical Abstract.

A scanning electron microscope coupled with energy-dispersive X-ray detector (EDX) (SEM Zeiss-LEO 440, Jena, Germany), is used for the microstructural array characterization. A X-ray diffractometer (Malvern Panalytical-X'Pert, Worcestershire, UK) operated under 40 kV and 30 mA, with Cu K α radiation and a wavelength of 0.15406 nm, was used to analyze/identify the constituent phases. The 2 θ range between 20° and 90° was used. The relative densities of the samples were obtained using the Archimedes method. For this purpose, a specific gravity measurement kit (SMK-401) from Shimadzu (10⁻⁴ g) (AUW220, Kyoto, Japan) was utilized. A universal electrohydraulic servo machine (Equilam-EQTB-100, Diadema, Brazil) with a speed-cross of approximately 25 mm.min⁻¹ and a strain rate of approximately 2 × 10⁻⁴ s⁻¹ was used. The tensile strength measurements were carried out using samples with a gauge size of ~25 mm according to the standard ASTM E8M/04 (American Society for Testing and Materials). The effects of natural aging for 210 days on the hardness values of the sintered samples were evaluated. Vickers hardness (HV) measurements using Buehler equipment (Wilson VH1102, Lake Bluff, IL, USA) according to ASTM E92 were carried out. At least 20 measurements were obtained for each of the sides of the samples examined. For this purpose, 9.8 N and a dwell time of 10 s were considered. The sizes of the particles were measured using ImageJ[®] software v. 1.8.0_172 (National Institutes of Health, Bethesda, MD, USA). To guarantee the reproducibility of the values examined, in all characterization techniques, the experiments were conducted in triplicate.

3. Results and Discussion

3.1. Powder Characterization

It is well known that the mechanical properties of alloys are affected by the initial sizes of the powders that control the sintering kinetics. The powder size affects the surface area. A number of small pores are produced by small particles in the entire part, as reported by Mostafaei et al. [19]. It is known that the hard-to-ductile particle ratio affects the resulting densification, as reported by Hafizpour and Simchi [20]. It has also been reported that there is an adequate size ratio, depending on the nature of the two or three distinct powders utilized that compose the composite examined [20–23]. Based on these assertions, in the present investigation, a “quasi” 1:1 size ratio is adopted. Thus, three distinct powders

(i.e., Al, Cu and Al₂O₃Zn) are considered. Additionally, this constitutes one limitation and restriction of this present study. To evaluate the effects of particle sizes on the experimental ultimate tensile strengths (UTS) of the Al₆Cu₅Zn alloy samples, the starting powders were analyzed. Four distinctive mesh ranges were evaluated, i.e., between 325 and 200 mesh (45 to 75 μm), 325 and 140 mesh (45 to 106 μm), 200 and 140 mesh (75 to 106 μm), and 140 and 100 mesh (106 to 150 μm). These mesh values (ASTM E11-17) were considered with 1:1 size ratios; the resulting UTS attained were 86 (\pm 11), 84 (\pm 16), 117 (\pm 5) and 68 (\pm 10) MPa, respectively. It is also worth noting that a sintering temperature of 600 $^{\circ}\text{C}$ for 1.5 h was adopted. Based on these experimental results, a 1:1 size ratio with a mesh ranging between 200 and 140 mesh was utilized.

Typical SEM micrographs of the starting powders of Al, Cu and Al₂O₃Zn to compose the blend of Al₆Cu₅Zn alloy are shown in Figure 1. The regular shapes and rough surfaces of Al powders are observed. This is commonly expected when milled powders are produced. The Cu powders show irregular shapes but a lower rough surface than the Al powders. This seems to be intimately associated with the higher ductility of Cu than Al. The morphology surfaces of the Al₂O₃Zn particles are similar to those of Al powders. However, the powder particles demonstrate some deformation lines, which are characteristics remaining from the milling applied. A typical SEM image of the mixture of the three powders is shown in Figure 1. Similar powder sizes are clearly evidenced (i.e., a size ratio of 1:1, independent of the considered powder nature). Cu powder particles are easily identified since their particles are brighter than other particles. This is evaluated by observing the backscattering electron (BSE) images using SEM characterization.

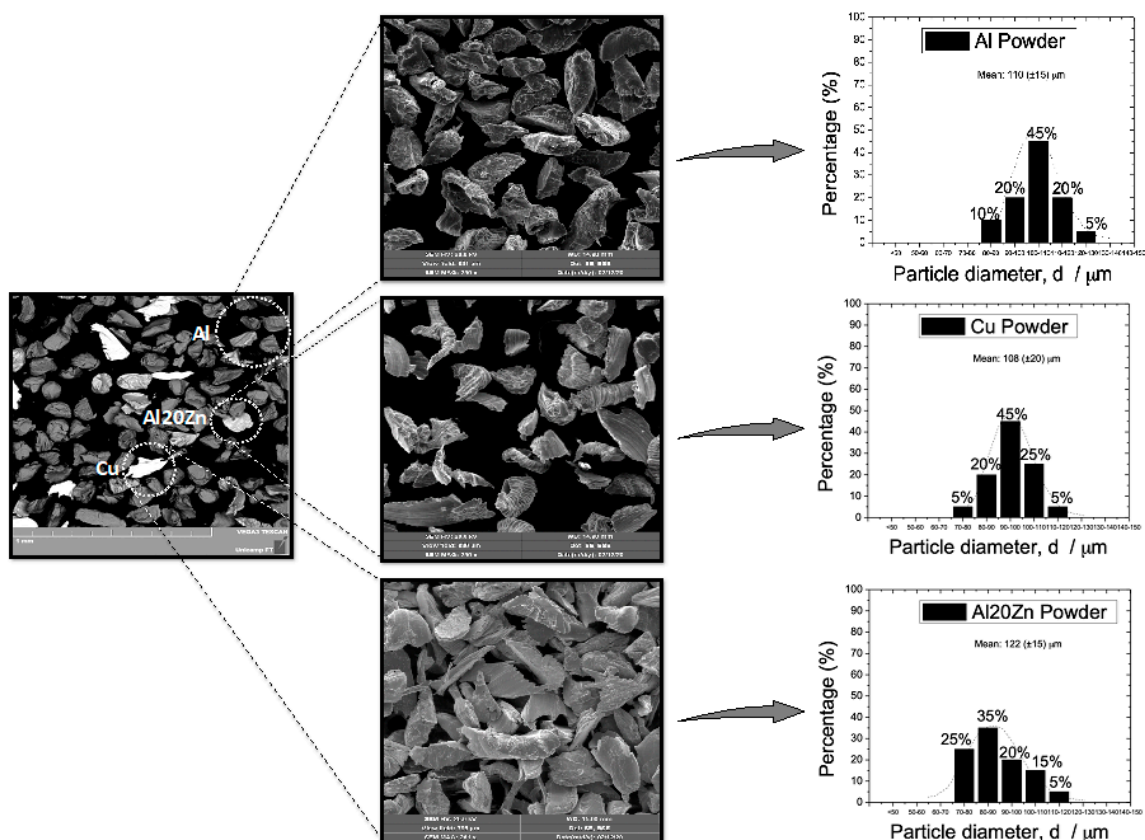


Figure 1. Typical SEM images of the morphology of Al, Cu, and Al₂O₃Zn powders and their blending to create the Al₆Cu₅Zn alloy (magnification of 250 \times).

Concomitant analysis of the microstructures and the engineering stress vs. strain curves (see the Supplementary Material) suggests that a reduction in UTS (68 \pm 10 MPa) is attained when the particle size is increased. Rudianto et al. [10] have reported that the sizes

of particles have critical roles in the UTS results. This is due to the powder characteristics strongly affecting the sinterability of the alloys. It is known that the larger particles are difficult to rearrange in the powders, and high porosity remains. This induces a high pore-solid interfacial area; consequently, the free energy of the system is also increased [24].

The UTS of 117 ± 5 MPa was obtained using particle sizes with a larger distribution range, with a particle size lower than $150 \mu\text{m}$. Özey, Gencer and Gökçe [6] have demonstrated that the irregular powder sizes facilitated the rearrangement among particles, and consequently, the porosity after sintering was decreased. It is worth noting that the selection of a pre-determined powder size range is under the strict control of the distribution curve. This constitutes a drawback, and the processing time is increased. Consequently, the final manufacturing cost also increased. It has also been reported that the space available inside the dies and the dislocation of powders depend on the morphology and size of the particles [25]. From the experimental observations, granulometry between 75 and $106 \mu\text{m}$ showed similar values for all the powder sizes (117 MPa). Lumley and Schaffer [26] obtained the best UTS results using the same particle size range (i.e., 75 - $106 \mu\text{m}$) when the Al-4Cu alloy is investigated.

3.2. Microstructural and Mechanical Properties

Since the highest UTS result is that of the range of the size particles between 200 and 140 mesh (75 - $106 \mu\text{m}$), all other subsequent heat treatments adopted this size of particle. The sintering temperatures at 585°C , 600°C and 615°C were carried out over 0.5 h. Typical XRD patterns are shown in Figure 2. Based on the experimental sintering temperatures, thermodynamic conditions for Al_2Cu intermetallic material are expected, as previously reported [22,23]. In fact, this is confirmed when the reflection peaks corresponding to the Bragg planes (110), (200), (211), (220), (112) and (310) at angles of $\sim 21^\circ$, 30° , 38° , 42° , 43° and $\sim 47^\circ$ were characterized (JCPDS file number # 01-1180). At angles of $\sim 38^\circ$, 44° , 64° , 78° and $\sim 83^\circ$ corresponding to the crystallographic planes (111), (200), (220), (311) and (222), respectively, peaks appeared that are associated with Al (JCPDS #00-001-1180), as also previously reported [18,22,23]. Since the powders produced from the as-cast Al20Zn alloy were also used to create the AlCuZn samples at an angle of approximately 41.5° , an overlapped peak seems to be correlated with the Zn-based solid solution. Zn-based $P6_3/mmc$, space group number 194, with reference code 98-024-7160, as also reported by Gogola et al. [27]. At $\sim 48^\circ$, another overlapped peak is associated with another plane (202) corresponding to Al_2Cu .

The densification values depend on both the sintering time and temperature, as confirmed in Figure 3. At a temperature range between 585°C and 615°C , in general, the densification increased with the increase in the sintering period. Using 0.5 h and 1.5 h of sintering, when a higher sintering temperature was provided, densification was increased. However, at 615°C , when a higher liquid portion was promoted, a slightly decreasing trend in the densification was observed. In addition, when a sintering time of 3 h was used, the three examined samples had very similar densification levels, as depicted in Figure 3. A similar effect was also reported previously when Al/Cu composites were sintered [22]. It was also found that the porosity tended to decrease with the increase in the sintering temperature. This was associated with the liquid phase filling the pores and migrating into the remaining vacancies among the interfaces of the compacted powders. Lee and Ahn [3] reported that densification increased with increasing temperature, and the diffusion increased. Consequently, the coalescence among the particles increased, and the porosity decreased.

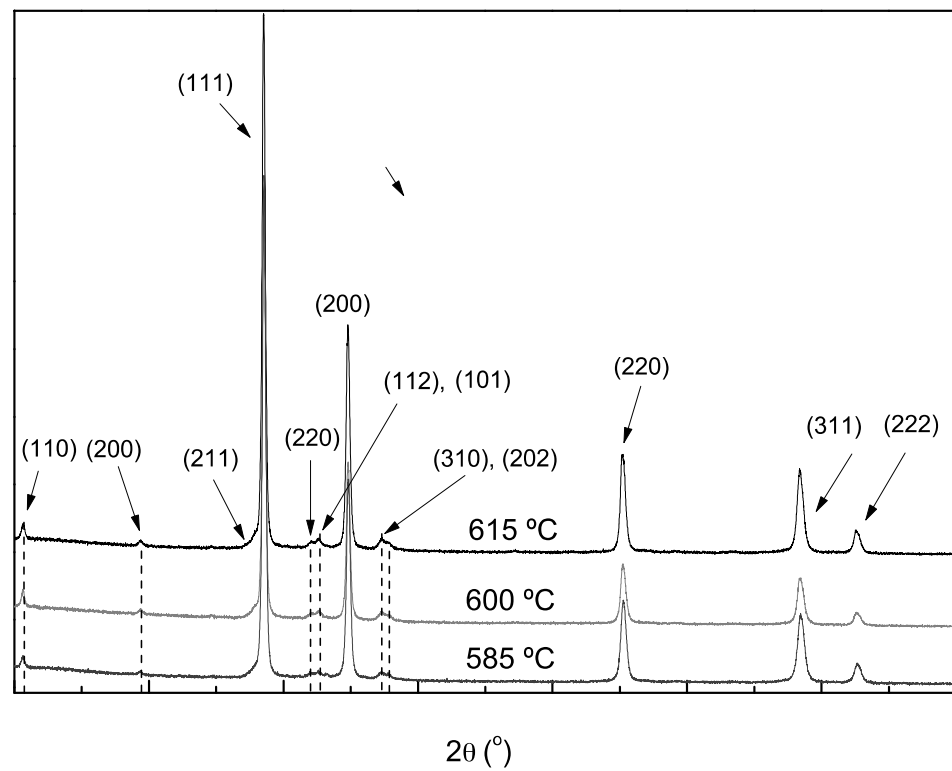


Figure 2. XRD patterns of the Al₆Cu₅Zn alloy at 0.5 h.

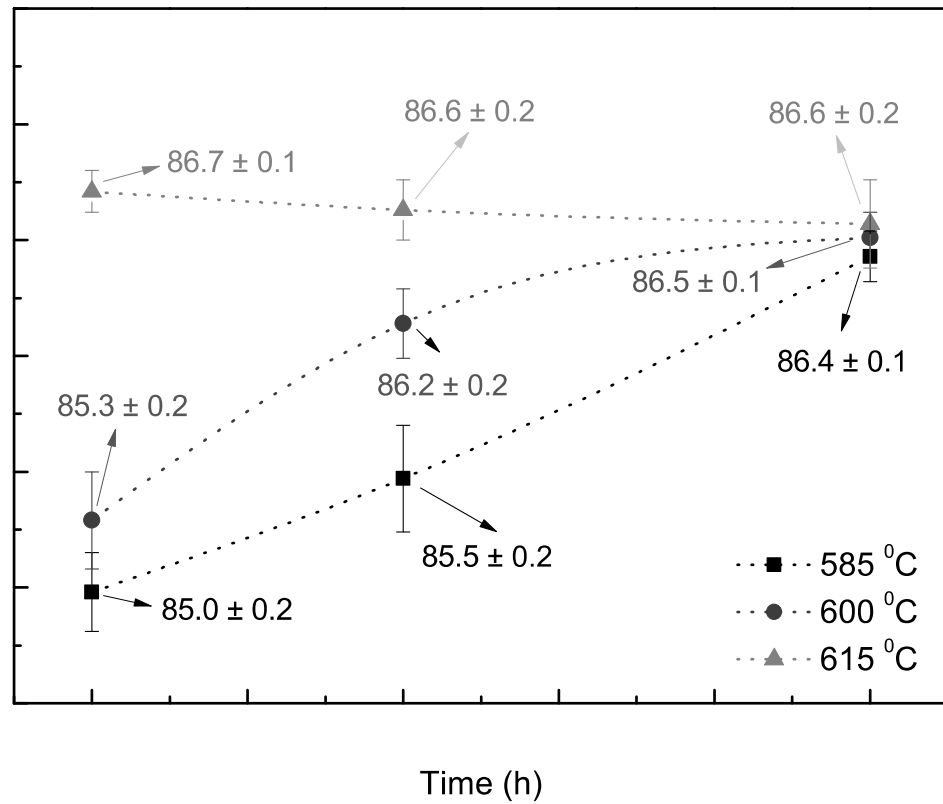


Figure 3. Densification for different temperatures and sintering times, obtained using the Archimedes method.

Typical SEM micrographs of the Al₆Cu₅Zn samples at three different sintering temperatures are shown in Figure 4. The decreasing trend of voids with increasing sintering temperature is evidenced (in the circles). It is clear that the lowest porosity level is that of the Al₆Cu₅Zn sample sintered at 615 °C for 0.5 h. Although it has not been systematically investigated, these pores seem to be associated with the remaining porosity when compacting at the powder stage. In addition, it is also possible that some specific voids or microvoids remained from a possible Kirkendall void constituent, mainly when sintering at 585 °C was carried out. It is noted that at this temperature, no liquid-assisted sintering was predominant. Özay, Gencer and Gökçe [6] reported that in their study, the liquid phase occurred and the diffusion mechanism accelerated. In addition, a possible thin layer of oxide on Al particles could be ruptured, and bonding bridges between the particles were provided.

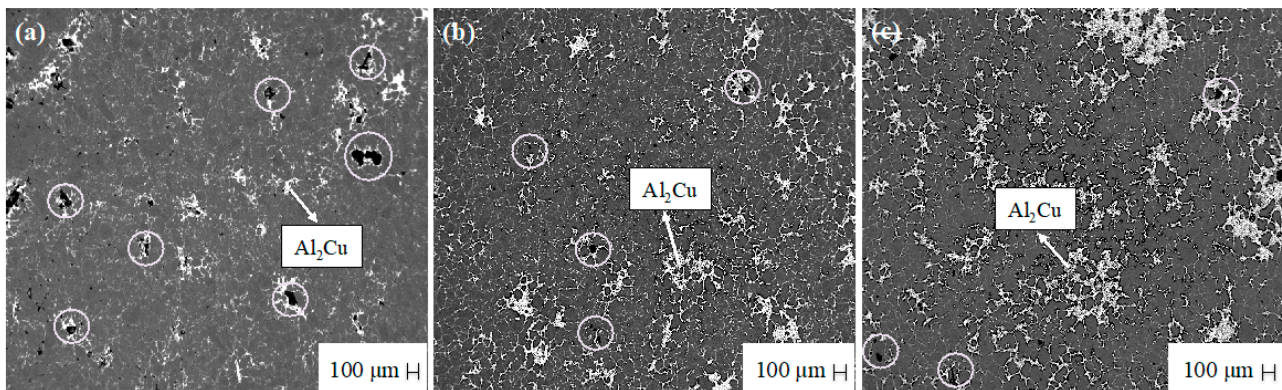


Figure 4. Typical SEM micrographs of the Al₆Cu₅Zn samples sintered for 0.5 h at: (a) 585 °C; (b) 600 °C; and (c) 615 °C.

The experimental results of the engineering stress vs. strain of the Al₆Cu₅Zn samples created at three distinct sintering temperatures are shown in Figure 5. Additionally, three different sintering times are demonstrated, i.e., 0.5 h, 1.5 h and 3 h. At the first analysis, it can be seen that during the three sintering periods, the samples sintered at 600 °C and 615 °C exhibited similar mechanical responses. At 615 °C, when a sintering time of 0.5 h is analyzed, the obtained UTS is approximately 80 MPa, while after 1.5 h and 3 h, the UTS values are ~104 and 125 MPa, respectively. Additionally, it can be seen that with the increase in the sintering period, the UTS increased, i.e., ~23% from 0.5 h to 1.5 h and ~17% from 1.5 h to 3 h (from 80 to 104 MPa and from 104 to 125 MPa, respectively).

Additionally, the worst UTS values are those of the Al₆Cu₅Zn samples sintered at 585 °C. This is correlated to the fact that no assisted liquid phase took place, as occurred with the other examined samples sintered at 600 and 615 °C (Figure 4). When the samples were sintered for 0.5 and 1.5 h, similar UTS values were reached. These observations are intimately associated with the selected sintering temperatures.

A Zn-Al phase diagram is shown in Figure 6a. Based on the chemical composition of the Al₂₀Zn powder, under equilibrium conditions, at 585 °C, a small amount of liquid was formed. In contrast, when the Al₆Cu₅Zn samples were sintered at 600 and 615 °C, a higher quantity of the liquid phase was formed. When the sintering period is increased, the liquid portion can be formed more easily, and it penetrates inside the voids and microvoids surrounding the powder particles. In this way, these possible microvoids (triggered by the Kirkendall effect) can be filled by the liquid phase (Figure 6b). It is also noted that Cu particles were also distributed throughout the bulk of the composite. Although Cu particles have a melting point (~1084 °C) that is substantially higher than the sintering temperatures adopted, their atomic diffusion is intense and is sufficient to migrate preferentially at Al grain boundaries, as schematically represented in Figure 6c. This has also been reported by other studies [23,28] when Al/Cu composites were sintered.

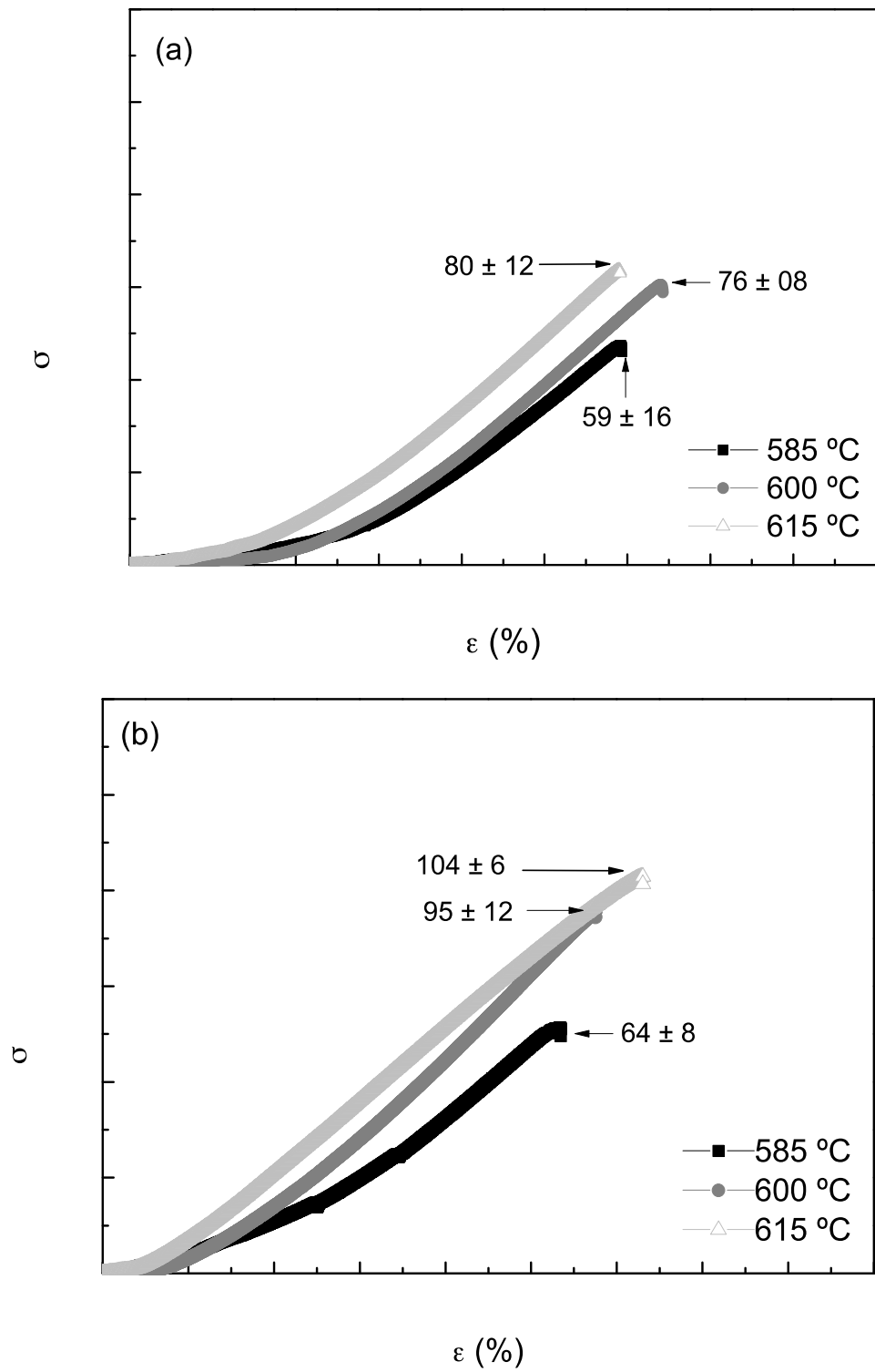


Figure 5. Cont.

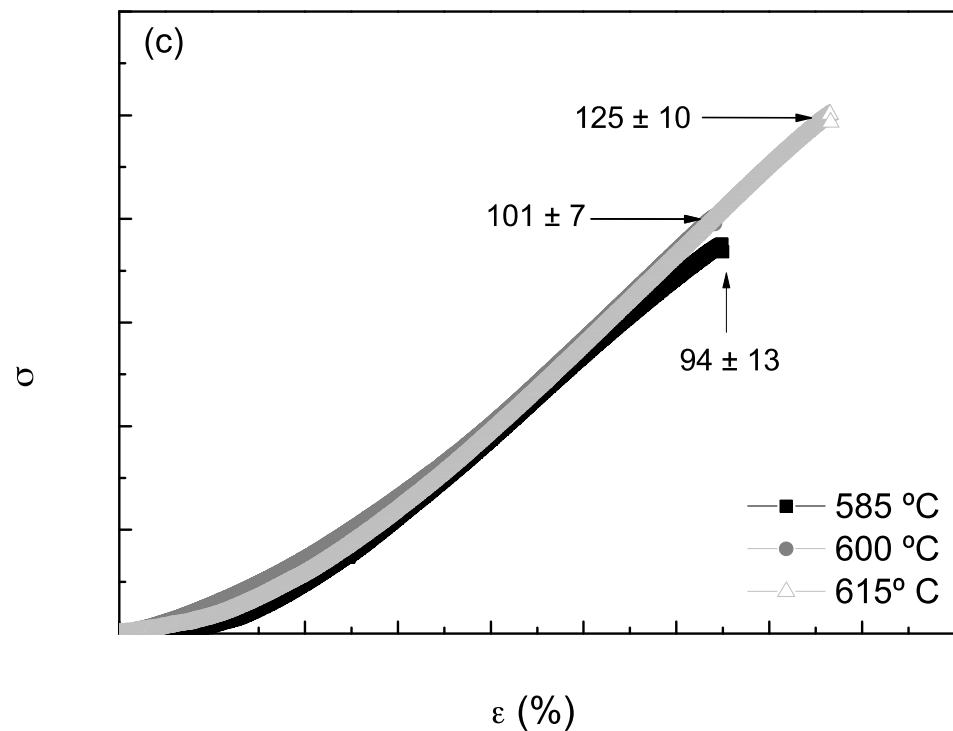


Figure 5. Experimental results of engineering stress-strain values as a function of both sintering time and temperature: (a) 0.5 h; (b) 1.5 h; and (c) 3 h.

It is also significant that when the Al₂₀Zn powder particles were liquefied, after complete solidification, a resulting as-cast microstructural dendritic array was formed. In this type of formation, the Cu particles are dissolved, and the as-cast Al₂₀Zn portion possibly reacts with the Cu and Zn contents, up to their solubility limits, which are diluted into the Al matrix. The low Zn concentration detected when the EDX analyses were carried out confirms this. When the obtained XRD and EDX partners were compared, we deduced that Zn constitutes a solid solution phase (η phase).

A typical micrograph of the Al₆Cu₅Zn sample sintered at 585 °C for 3 h and the corresponding EDX analysis are shown in Figure 7a. The elemental Cu (white regions) was not completely consumed, as can be observed in the EDX intensity peaks. The EDX peaks associated with Cu and Al also indicate that intermetallic Al₂Cu has formed (ratio of ~1:2). These are neighboring Cu particles as well as in regions possibly constituted by crystallographic Al grains and at powder interfaces. It has been demonstrated that intermetallic phase formation significantly improves the mechanical properties of the resulting material [29–32]. The EDX peak corresponding to Zn content is also characterized. From the metallurgical point of view, under equilibrium conditions, Zn content with liquid (L) and solid phase attains levels of approximately 5 wt %. The observed Zn content supported this finding, although in the experiments, a nonequilibrium condition had occurred. Additionally, it seems that a η -phase (Zn-based) solid solution phase was formed, as previously reported by Gogola et al. [27], as suggested by both the EDX and XRD results. Figure 7b shows the typical micrographs and EDX analyses of the Al₆Cu₅Zn sample, sintered at both 585 °C and 615 °C over 3 h. An increase in the Al₂Cu content was observed when the samples were created under these conditions.

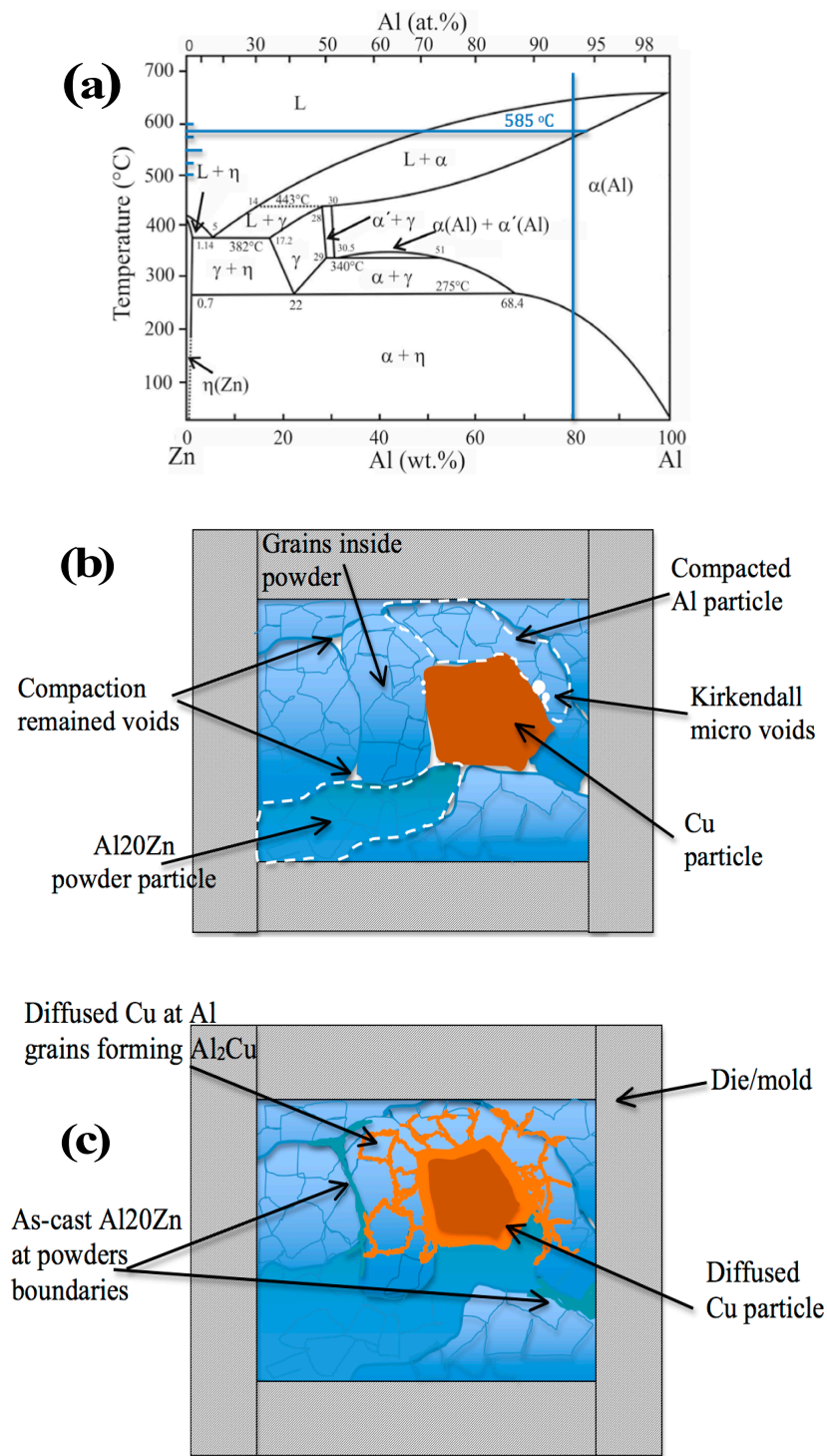


Figure 6. (a) Binary Zn-Al phase diagram; (b) schematic representation of the compacted and sintered powders at 585 °C; (c) evidence of the diffused Cu particles forming Al₂Cu intermetallic constituents and the accommodation of liquid phase (as-cast) boundary powder particles.

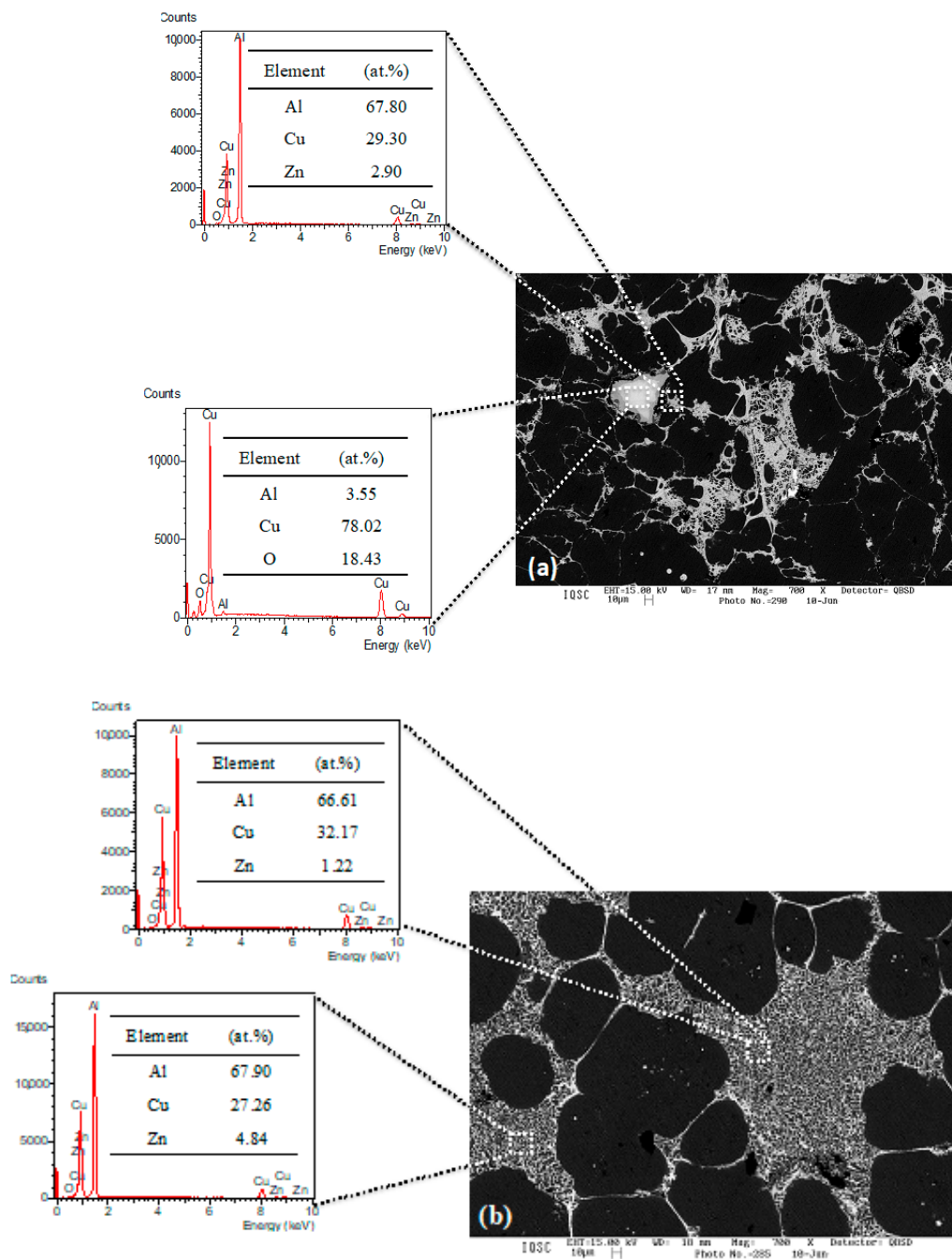


Figure 7. Typical SEM and EDX results of the Al₆Cu₅Zn alloy at: (a) 585 °C for 3 h, revealing distinct Al₂Cu and Cu-rich regions, respectively; and (b) 615 °C for 3 h also evidenced a substantial region rich in Al₂Cu (~65 and 70 wt % Al and ~24 and 28 wt % Cu contents).

3.3. Natural Aging Results

Natural aging is a spontaneous phenomenon seen in a supersaturated solid solution formed during room-temperature heat treatment. Due to the high number of retained atoms in the solid solution after rapid cooling, the hardening of naturally aged alloys was achieved, as reported by Zhao et al. [33]. This occurs due to the GP zones homogeneously nucleating into the matrix (as thin plate-like shapes). During the natural aging of Al alloys, the observed increase in the attained hardness values is related to the formation of GP zones; at temperatures below 100 °C, no other phases are formed.

Figure 8 shows the variations in hardness with the aging of the Al₆Cu₅Zn alloy over 210 days. It is verified that during the initial 10 days, the hardness increased from ~77 to

~85 HV. This can be attributed to the formation of the GP zones precursor to the metastable phase, which undergoes gap-controlled diffusion, as reported by Ogura et al. [34]. This mechanism is possibly due to the high retention of gaps, promoted by the water-quenching that was used. In the case of an aging period longer than 120 days, the majority of solute precipitation has already occurred. A trend regarding stabilized hardness was observed, as shown in Figure 8. Similar behavior was also observed when the separate aging periods of an Al7050 alloy were investigated [35].

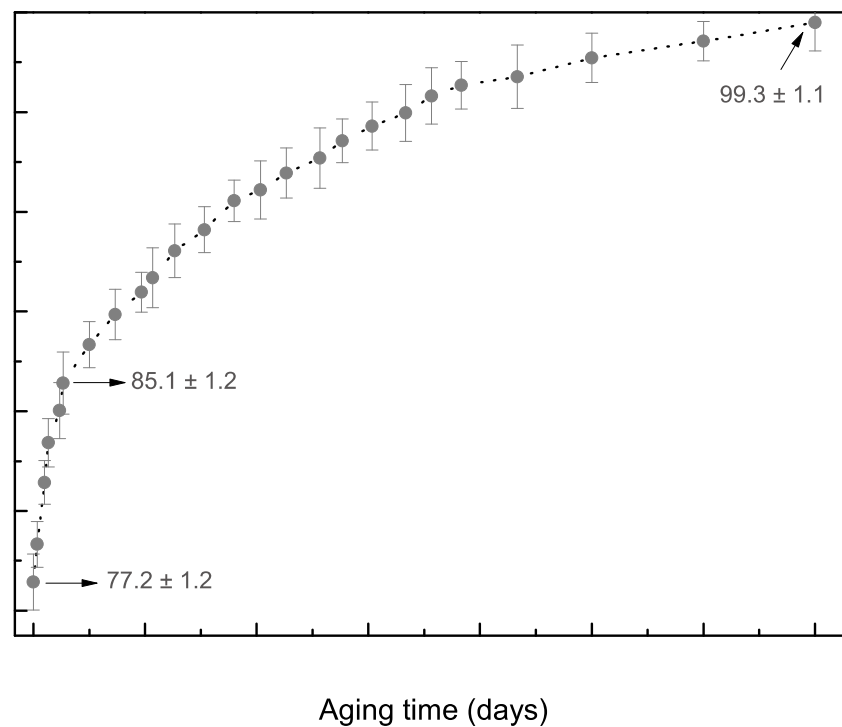


Figure 8. Variation in the hardness of the Al₆Cu₅Zn as a function of the natural aging process.

Binary Al-Cu alloys have relatively stable mechanical properties after a few days. The amount of Zn in the Al-Cu alloy affects the stability at room temperature, and it also contributes to an increase in mechanical properties over the years [36,37]. The formation of the Al₄Cu₃Zn phase was induced when Zn content was included, when a peritectic reaction between the liquid phase and Al-Cu was prevalent. The above-mentioned phase was formed between 500 and 600 °C; stability occurred at ~300 °C [8,38]. Cardenas et al. [39] have demonstrated that the Al₄Cu₃Zn phase has a beneficial effect on the hardness of Zn-Al-Cu alloys. The Al₄Cu₃Zn phase was not identified in the experimental results of the XRD patterns. As mentioned above, a Zn-based solution is more likely to occur.

In order to predict the mechanical behavior of the produced material, a mathematical model using nonlinear regression analysis was used. Hardness with aging time can be determined by using the following Equation (1):

$$\text{Hardness (HV)} = 100.43 - 6.69 \frac{-x}{3.51} - 8.86 \frac{-x}{74.93} - 8.71 \frac{-x}{74.94} \quad (1)$$

It can be seen that the hardness tends to stabilize over time, probably at 500 days (~100 HV). Although a decreasing tendency in the hardness is attributed to the over-aging occurring in Al-Cu-based alloys, based on the proposed Equation (1), it is not possible to predict this occurrence. From the above experimental results, it can be observed that the mechanical behavior (UTS) and hardness of the Al₆Cu₅Zn alloy are similar to those of the as-cast Al alloys [40–45]. This suggests that the proposed alloy and the adopted liquid-assisted sintering are promising as a manufacturing route. They offer both environmentally friendly and economical aspects (no foundry manufacturing is needed and recycled powder

or rejected material from rolling can be utilized). Besides these advantages, low energy consumption without the need for a melting point is possible.

4. Conclusions

This investigation is focused on the microstructural and mechanical characterization of a noncommercial Al₆Cu₅Zn alloy, which is manufactured by using liquid-assisted sintering. From the experimental results, the following conclusions can be drawn:

1. The selection of the particle sizes provided powder sizes ranging between 200 and 140 mesh; with these sizes, the best UTS values were attained.
2. Regarding this same particle size, when associated with a compaction pressure of 364 MPa, a densification level of approximately 85% was attained.
3. From the separate sintering temperatures and times, it was found that UTS of 125 MPa was reached when sintering at 615 °C for 3 h is used. This value is similar to that of the as-cast Al-Cu-based alloys (produced without heat treatment). Additionally, it is also suggested that the hardness, after natural aging for 500 days, reached approximately 99 HV. With these attained mechanical properties, the Al and Cu elemental powders are associated with Al-Zn powder to constitute an Al₆Cu₅Zn alloy with some advantages, such as low energy consumption and a reduction in the metal fumes commonly produced by foundries.

Supplementary Materials: The following supporting information can be downloaded at: <https://www.mdpi.com/article/10.3390/met12060962/s1>, Figure S1: Experimental results of engineering stress-strain values as a function of the size of particles.

Author Contributions: The authors would like to emphasize the individual contributions of each author: E.L.O.—alloy manufacture, acquisition and data curation; W.R.O.—review of the data, validation of morphology results, drafting the manuscript A.D.B.—data curation of scanning electron microscopy and X-ray diffraction, drafting the manuscript; G.S.P.—main researcher, SEM/EDX analyses, editing assistance, monitoring of the main analyzes, drafting the manuscript. All authors have read and agreed to the published version of the manuscript.

Funding: This research was funded by the CNPq (310010/2020-9), FAPESP (2013/12729-5, 2016/13352-0); and CAPES (Eder Lopes Ortiz master fellowship).

Institutional Review Board Statement: Not applicable.

Informed Consent Statement: Not applicable.

Data Availability Statement: The authors also declare that all research data supporting this publication are directly available within this publication.

Conflicts of Interest: The authors declare no conflict of interest.

References

1. Stojanovic, B.; Bukvic, M.; Epler, I. Application of aluminum and aluminum alloys in engineering. *Appl. Eng. Lett.* **2018**, *3*, 52–56. [[CrossRef](#)]
2. Zhu, Y.; Sun, K.; Frankel, G.S. Intermetallic phases in aluminum alloys and their roles in localized corrosion. *J. Electrochem. Soc.* **2018**, *165*, C807–C820. [[CrossRef](#)]
3. Lee, S.H.; Ahn, B. Effect of compaction pressure and sintering temperature on the liquid phase sintering behavior of Al–Cu–Zn alloy. *Arch. Metall. Mater.* **2015**, *60*, 158–162. [[CrossRef](#)]
4. Chak, V.; Chattopadhyay, H.; Dora, T.L. A review on fabrication methods, reinforcements and mechanical properties of aluminum matrix composites. *J. Manuf. Process.* **2020**, *56*, 1059–1074. [[CrossRef](#)]
5. Bonatti, R.S.; Siqueira, R.R.; Padilha, G.S.; Bortolozzo, A.D.; Osório, W.R. Distinct Al_p/Si_p composites affecting its densification and mechanical behavior. *J. Alloys Compd.* **2018**, *757*, 434–447. [[CrossRef](#)]
6. Özay, Ç.; Gencer, E.B.; Ökçe, G. Microstructural properties of sintered Al–Cu–Mg–Sn alloys. *J. Therm. Anal. Calorim.* **2018**, *134*, 23–33. [[CrossRef](#)]
7. Naeem, H.T.; Mohammed, K.S.; Ahmad, K.R. The role of cobalt and nickel intermetallic phases on the mechanical properties and microstructure evolution of Al–Zn–Mg–Cu alloys. *Mater. Res.* **2014**, *17*, 1663–1676. [[CrossRef](#)]
8. Liang, S.-M.; Schmid-Fetzer, R. Thermodynamic assessment of the Al–Cu–Zn system, part II: Al–Cu binary system. *Calphad Comput. Coupling Phase Diagr. Thermochem.* **2015**, *51*, 252–260. [[CrossRef](#)]

9. Hou, W.T.; Shi, J.T.; Hou, L.G.; Zhang, J.S. An improved thermo–mechanical treatment of high-strength Al–Zn–Mg–Cu alloy for effective grain refinement and ductility modification. *J. Mater. Process. Technol.* **2017**, *239*, 303–314.
10. Rudianto, H.; Jang, G.J.; Yang, S.S.; Kim, Y.J.; Dlouhy, I. Evaluation of sintering behavior of premix Al–Zn–Mg–Cu alloy powder. *Adv. Mater. Sci. Eng.* **2015**, *15*, 1–8. [[CrossRef](#)]
11. Hatch, J.E. *Aluminum: Properties and Physical Metallurgy*; ASM International: Metals Park, OH, USA, 1984.
12. Martin, J.W. *Precipitation Hardening*, 2nd ed.; Butterworth–Heinemann: Oxford, UK, 1998.
13. Byrne, J.G.; Fine, M.E.; Kelly, A. Precipitate hardening in an aluminium–copper alloy. *Philos. Mag. J. Theor. Exp. Appl. Phys.* **1961**, *6*, 1119–1145. [[CrossRef](#)]
14. Poole, W.J.; Embury, J.D.; Lloyd, D.J. *Fundamentals of Aluminium Metallurgy*; Woodhead Publishing Series in Metal and Surface Engineering; Woodhead Publishing: Thorston, UK, 2011; pp. 307–344.
15. Ngugi, J.; Rading, G.O.; Odera, B.O.; Ngobe, B.; Forbes, R.; Cornish, L.A. Partial isothermal sections of the Cu–rich corner of the Al–Cu–Zn system at 200 and 240 °C. *J. Phase Equilibria Diffus.* **2019**, *40*, 588–599. [[CrossRef](#)]
16. Rana, R.S.; Purohit, R.; Das, S. Reviews on the influences of alloying elements on the microstructure and mechanical properties of aluminum alloys and aluminum alloy composites. *Int. J. Sci. Res.* **2012**, *2*, 1–7.
17. Pournaderi, S.; Akhlaghi, F. Wear behaviour of Al6061–Al2O3 composites produced by in-situ powder metallurgy (IPM). *Powder Technol.* **2017**, *313*, 184–190. [[CrossRef](#)]
18. Elias, A.L.P.; Koizumi, M.S.; Ortiz, E.L.; Rodrigues, J.F.Q.; Bortolozzo, A.D.; Osório, W.R.; Padilha, G.S. Corrosion behavior of an Al–Si casting and a sintered Al/Si composite immersed into biodiesel and blends. *Fuel Process. Technol.* **2020**, *202*, 106360. [[CrossRef](#)]
19. Mostafaei, A.; De Vecchis, P.R.; Nettleship, V.; Chmielus, M. Effect of powder size distribution on densification and microstructural evolution of binder–jet 3D–printed alloy 625. *Mater. Des.* **2019**, *162*, 375–383. [[CrossRef](#)]
20. Hafizpour, H.R.; Simchi, A. Investigation on compressibility of Al–SiC composite powders. *Powder Metall.* **2008**, *51*, 217–223. [[CrossRef](#)]
21. Bouvard, D. Densification behaviour of mixtures of hard and soft powders under pressure. *Powder Technol.* **2000**, *111*, 231–239. [[CrossRef](#)]
22. Meyer, Y.A.; Bonatti, R.S.; Costa, D.; Bortolozzo, A.D.; Osório, W.R. Compaction pressure and Si content effects on compressive strengths of Al/Si/Cu alloy composites. *Mater. Sci. Eng. A* **2020**, *770*, 1385747. [[CrossRef](#)]
23. Satizabal, L.M.; Caurin, H.F.N.; Meyer, Y.A.; Padilha, G.P.; Bortolozzo, A.D.; Osório, W.R. Distinct heat treatments and powder size ratios affecting mechanical behavior of Al/Si/Cu composites. *J. Compos. Mater.* **2021**, *55*, 3589–3605. [[CrossRef](#)]
24. Su, K.P.; Chen, X.X.; Wang, O.; Huo, D.X.; Liu, Z.W. Effect of milling on the structure and magnetic properties in Mn54Al46 flakes prepared by surfactant–assisted ball milling. *Mater. Charact.* **2016**, *114*, 263–266. [[CrossRef](#)]
25. Pulido-Suárez, P.A.; Uñate-González, K.S.; Tirado-González, J.G.; Esquerra-Arce, A.; Esquerra-Arce, J. The evolution of the microstructure and properties of ageable Al–Si–Zn–Mg alloy during the recycling of milling chips through powder metallurgy. *J. Mater. Res. Technol.* **2020**, *9*, 11769–11777. [[CrossRef](#)]
26. Lumley, R.N.; Schaffer, G.B. The effect of additive particle size on the mechanical properties of sintered aluminium–copper alloys. *Scr. Mater.* **1998**, *39*, 1089–1094. [[CrossRef](#)]
27. Gogola, P.; Gabalcová, Z.; Suchánek, H.; Babinec, M.; Bonek, M.; Kusý, M. Quantitative X–ray diffraction analysis of Zn–Al based alloys. *Arch. Metall. Mater.* **2020**, *65*, 959–966.
28. Ogel, B.; Gurbuz, R. Microstructural characterization and tensile properties of hot pressed Al–SiC composites prepared from pure Al and Cu powders. *Mater. Sci. Eng. A* **2001**, *301*, 213–220. [[CrossRef](#)]
29. Adeosun, S.O.; Balogun, S.A.; Osoba, L.O.; Ayoola, W.A.; Oladoye, A.M. Effect of Cu and Zn addition on the mechanical properties of structural aluminum alloy. *Int. J. Mod. Manuf. Technol.* **2011**, *3*, 103–110.
30. Engin, S.; Büyük, U.; Maraşlı, N. The effects of microstructure and growth rate on microhardness, tensile strength, and electrical resistivity for directionally solidified Al–Ni–Fe alloys. *J. Alloys Compd.* **2016**, *660*, 23–31. [[CrossRef](#)]
31. Matli, P.R.; Fareeha, U.; Shakoor, R.A.; Mohamed, A.M.A. A comparative study of structural and mechanical properties of Al–Cu composites prepared by vacuum and microwave sintering techniques. *J. Mater. Res. Technol.* **2018**, *7*, 165–172. [[CrossRef](#)]
32. Ebhota, W.S.; Jen, T.-C. Formation and Their Effect on Mechanical Properties of Al–Si–X Alloys. In *Intermetallic Compounds–Formation and Applications*; Aliofkhaezai, M., Ed.; BoD–Books on Demand: Nordstedt, Germany, 2018.
33. Zhao, J.; Liu, Z.; Bai, S.; Zeng, D.; Luo, L.; Wang, L. Effects of natural aging on the formation and strengthening effect of G.P. zones in a retrogression and re–aged Al–Zn–Mg–Cu alloy. *J. Alloys Compd.* **2020**, *829*, 154469. [[CrossRef](#)]
34. Ogura, T.; Hirokawa, S.; Cerezo, A.; Sato, T. Atom probe tomography of nanoscale microstructures within precipitate free zones in Al–Zn–Mg(–Ag) alloys. *Acta Mater.* **2010**, *58*, 5714–5723. [[CrossRef](#)]
35. Buha, J.; Lumley, R.N.; Crosky, A.G. Secondary ageing in an aluminum alloy 7050. *Mater. Sci. Eng. A* **2008**, *25*, 1–10. [[CrossRef](#)]
36. Chen, H.; Xin, X.; Dong, D.Y.; Ren, Y.P.; Hao, S.M. Study on the stability of the T' phase in the Al–Zn–Cu ternary system. *Acta Metall. Sin.* **2004**, *17*, 269–273.
37. Abolfazl, A.; Taheri, A.K.; Taheri, K.K. Recent advances in ageing of 7xxx series aluminum alloys: A physical metallurgy perspective. *J. Alloys Compd.* **2019**, *781*, 945–983.
38. Zobac, O.; Kroupa, A.; Richter, K.W. Experimental study of the Al–Cu–Zn ternary phase diagram. *J. Mater. Sci.* **2020**, *55*, 10796–10810. [[CrossRef](#)]

39. Villegas–Cardenas, J.D.; Saucedo–Muñoz, M.L.; Lopez–Hirata, V.M.; Dorates–Rosales, H.J.; Gonzalez-Velazquez, J.L. Effect of phase transformations on hardness in Zn–Al–Cu alloys. *Mater. Res.* **2014**, *17*, 1137–1144. [[CrossRef](#)]
40. Casting. In *ASM Handbook*; ASM International: Almere, The Netherlands, 2008; Volume 15, p. 105.
41. Kurz, W.; Fisher, D.J. *Fundamentals of Solidification*; Trans Tech Public: Aedermannsdorf, Switzerland, 1992.
42. Shabestari, S.G.; Moemeni, H. Effect of copper and solidification conditions on the microstructure and mechanical properties of Al–Si–Mg alloys. *J. Mater. Processing Technol.* **2004**, *153–154*, 193–198. [[CrossRef](#)]
43. Xu, D.F.; Chen, K.H.; Chen, Y.Q.; Chen, S.Y. Evolution of the second–phase particles and their effect on tensile fracture behavior of 2219 Al–xCu alloys. *Metals* **2020**, *10*, 197. [[CrossRef](#)]
44. Song, Z.X.; Li, Y.D.; Liu, W.J.; Yang, H.K.; Cao, Y.J.; Bi, G.L. Effect of La and Sc Co–addition on the mechanical properties and thermal conductivity of as–cast Al–4.8% Cu alloys. *Metals* **2021**, *11*, 1866. [[CrossRef](#)]
45. Kang, H.J.; Park, J.Y.; Choi, Y.S.; Cho, D.H. Influence of the solution and artificial aging treatments on the microstructure and mechanical properties of die–cast Al–Si–Mg alloys. *Metals* **2022**, *12*, 71. [[CrossRef](#)]